IOP Publishing | International Atomic Energy Agency Nuclear Fusion
Nucl. Fusion **62** (2022) 086031 (10pp) https://doi.org/10.1088/1741-4326/ac6f67

Effect of electron temperature anisotropy on TEM in reversed-field-pinch plasmas

Y. Yao[1], T.C. Liu[1], S.F. Liu[1,*], K.E. Zhu[1], W. Kong[2,*], J.C. Li[3] and J.Q. Dong[4]

[1] School of Physics, Nankai University, Tianjin 300071, China
[2] College of Science, Civil Aviation University of China, Tianjin 300300, China
[3] Department of Earth and Space Sciences, Southern University of Science and Technology, Shenzhen 518055, China
[4] Southwestern Institute of Physics, Chengdu 610041, China

E-mail: lsfnku@nankai.edu.cn and wkong@cauc.edu.cn

Received 17 February 2022, revised 20 April 2022
Accepted for publication 13 May 2022
Published 23 June 2022

Abstract

For the first time in the reversed-field-pinch configuration, trapped electron mode (TEM) with anisotropies of electron temperature and its gradient is studied by solving the gyrokinetic integral eigenmode equation. Detailed numerical analyses indicate that TEM is enhanced by the anisotropy with temperature in the direction perpendicular to the magnetic field that is higher than that in the direction parallel to the magnetic field when the latter is kept constant. However, the enhancement is limited, such that TEM is weakened and even stabilized when the anisotropy is higher than a critical value, due to strong Landau damping. In comparison with the isotropic case, the lower Landau damping with the higher parallel electron temperature makes TEM instability easier to excite, which expands the TEM unstable region in the diagram of density and temperature scale lengths. In addition, it is found that the electron temperature gradient in the perpendicular direction offers a stronger driving force on TEM instability than that in the parallel direction. The overall effects of the temperature gradients of electrons and ions, magnetic shear, safety factor and density gradient on TEM in the presence of the anisotropies are presented in detail.

Keywords: reversed-field-pinch plasmas, gyrokinetic theory, trapped electron mode, anisotropies of electron temperature and its gradient

(Some figures may appear in colour only in the online journal)

1. Introduction

Microturbulence has always been a research focus in fusion plasmas [1, 2]. In particular, ion temperature gradient (ITG) instability has been proved to be the primary contributor causing anomalous transport in the core of tokamak plasmas in theory and experiments. As one of the types of electron drift waves, trapped electron mode (TEM) is driven by a trapped electron pressure gradient (electron density gradient and/or electron temperature gradient), and offers an important effect on electron anomalous transport. However, most of the former studies were performed with isotropic plasmas. In fact, plasma anisotropy is a common phenomenon, especially in space plasmas [3], where the anisotropy of electron temperature in solar wind has been clearly detected. In fusion plasmas, the phenomena of plasma anisotropy in xperiments have also been found with the application of various heating and current drive schemes [4–6], such as neutral beam injection and ion/electron cyclotron resonance heating (ICRH/ECRH). Moreover, the anisotropy of electron temperature directly acts on the bootstrap current, which is closely related to the steady-state scenario in fusion experiments, and has been wildly studied in tokamaks [7], stellarators [8] and reversed-field-pinch (RFP) plasmas [9]. Therefore, it is necessary to discuss the characteristics of microturbulence in anisotropic fusion plasmas.

* Authors to whom any correspondence should be addressed.

The first theoretical research on ITG mode in anisotropic plasmas can be traced back to 1988 [10]. Following this, local kinetic theory and full kinetic theory [11–14] were routine approaches used to discuss the effects of anisotropy in slab and toroidal tokamak plasmas. All the results showed that the higher ion temperature in the perpendicular direction to the magnetic field had an overall stabilization effect on ITG mode. But the conclusion was just the opposite for TEM in tokamak plasmas, where the higher perpendicular temperature enhanced TEM instability in certain anisotropic strengths, as shown in gyrokinetic theory [15] and simulation with the code GKNET [16].

With regard to RFP plasmas, study concerning the anisotropy remains elusive due to the RFP configuration characteristics. Firstly, most of the previous efforts were devoted to magnetohydrodynamic (MHD) chaos for the dynamo generation. Secondly, RFP theory shows that it can only rely on ohmic heating to heat plasmas; therefore, the demand for auxiliary heating is relatively small. Until the so-called quasi-single helicity or quasi-single axis state appeared in RFP experiments, indicating that the plasma inside the core is better confined and close to similar tokamak levels [17, 18], it had been recognized that the study of microturbulence in RFP plasmas requires more attention. On the other hand, anisotropic phenomena have also appeared in RFP experiments. For example, the EXTRAP-T2 experiment [19] showed that the ions were heated primarily in the direction parallel to the magnetic field, and the Madison symmetric torus (MST) experiment had to consider the plasma to be nearly isotropic after sawtooth crash heating [20]. The first study of microturbulence in an RFP can be traced back to 2008 [21], and then gyrokinetic theory [22–24] and simulation codes [25, 26] further discussed the characteristics of ITG mode and TEM in an RFP. All the results show that microturbulence in RFP plasmas is more stable than those in similar tokamak plasmas, since the Landau damping is stronger in the former. However, the results also show that ITG turbulence may be an important contributor to the total heat transport in RFP helical states [27], and the strong temperature gradient's microtearing instability may be the dominant turbulent mechanism [28]. Moreover, the influence of TEM-driven zonal flow on turbulence has been investigated [29, 30], and TEM has been further observed in MST experiments [31]. All these phenomena reveal that the study of microturbulence is equally important to understand the anomalous transport in RFP plasmas. Until now, no relative work on microturbulence in anisotropic RFP plasmas has been reported. Therefore, in this work, an integral eigenmode equation, retaining full ion kinetic effects and trapped electron nonadiabatic response, is derived from the linear gyrokinetic equation under the electrostatic limit in RFP plasmas, where the anisotropies of electron temperature and its gradient are taken into account. Furthermore, the numerical simulation code HD7 (a solver of the integral eigenmode equation), which has been used for ITG and TEM study in RFPs [22–24], is adopted and updated. The HD7 code has been widely used in slab [32] and tokamak [33, 34] plasmas to discuss the characteristics of microturbulence, and gotten well benchmark with some simulation codes [35]. Therefore, the influence of the anisotropies of electron temperature and its gradient on TEM can be presented in detail and compared with those in isotropic RFP and similar tokamak plasmas.

The remainder of this work is organized as follows. In section 2, the integral eigenmode equation is given. The numerical results are presented and analyzed in section 3. Section 4 is devoted to the conclusions and discussion.

2. Integral eigenvalue equation

In a toroidal plasma configuration, the magnetic field is usually expressed by the toroidal and poloidal components B_φ and B_θ as,

$$\mathbf{B} = B_\theta \mathbf{e}_\theta + B_\varphi \mathbf{e}_\varphi.$$

In RFP and tokamak configurations, the magnetic fields possess different features, such as $B_\theta \approx B_\varphi$ in an RFP while $B_\theta \ll B_\varphi$ in a tokamak, which has to be considered in studies. For example, the poloidal magnetic field B_θ must be taken into account in the total magnetic field in an RFP, $B = \sqrt{B_\theta^2 + B_\varphi^2} = B_\varphi\sqrt{1+\varepsilon^2/q^2} = B_\varphi \alpha$, where $\alpha = \sqrt{1+\varepsilon^2/q^2}$ with the safety factor q and inverse aspect ratio $\varepsilon = r/R$. But it is often ignored in a tokamak, $B \approx B_\varphi$. Moreover, the B_θ effect leads to $q < 1$ in an RFP, while $q > 1$ in a tokamak.

The quasi-neutrality condition $n_\mathrm{e} = n_\mathrm{i}$ is the basic equation used to describe the low-frequency electrostatic perturbation $\tilde{\phi}$ in hydrogen plasmas. The density of the charged particle n_j ($j = \mathrm{i}, \mathrm{e}$) includes the equilibrium density n_{j0} and perturbation density $\tilde{n}_j$, where $\tilde{n}_j$ consists of adiabatic and nonadiabatic responses of charged particles. In an axisymmetric toroidal geometry, it can be written as

$$\tilde{n}_j = -\frac{Q_j n_{j0}}{T_j}\tilde{\phi} + \int \mathrm{d}^3 v J_0(\zeta)\delta\tilde{H}_j.$$

Here, the nonadiabatic function $\delta\tilde{H}_j$ is obtained directly from the linear gyrokinetic equation of the charged particle [21], meaning that TEM driven by the electron temperature gradient is the main research object in this work.

$$\left[\frac{v_\parallel}{Rq\alpha}\partial_x - \mathrm{i}\left(\omega - \omega_{\mathrm{d}j}\right)\right]\delta\tilde{H}_j = -\mathrm{i}\left(\omega - \omega_*^j\right)J_0(\zeta) \times \frac{Q_j F_{Mj}}{T_j}\tilde{\phi}(x), \tag{1}$$

where Q_j, T_j and m_j are the charge, temperature and mass of the particle species j, respectively. Here, F_{Mj} is the Maxwell equilibrium distribution, R is the major radius and $v_\parallel$ is the particle's velocity along the magnetic field. Meanwhile, $J_0(\zeta)$ is the Bessel function of the zeroth order with $\zeta^2 = k_\perp^2 v_{tj}^2/\Omega_j^2$, $v_{tj}^2 = 2T_j/m_j$, $\Omega_j = eB/m_j c$ and $k_\perp$ is the wave number in the direction perpendicular to the magnetic field. Finally, $\omega_{\mathrm{d}j}$ and ω_*^j represent the effects of magnetic field drifts and plasma inhomogeneous profiles, respectively.

2.1. Trapped electron response

This work is devoted to the study of the effect of anisotropies of electron temperature and its temperature gradient on TEM. The nonadiabatic response of trapped electrons is obtained by solving the gyrokinetic equation of trapped electrons, and the passing electrons are adiabatic.

Firstly, the anisotropy of electron temperature is introduced in the Maxwell distribution function of electrons in velocity space,

$$F_{Me} = \left(\frac{m_e}{2\pi}\right)^{\frac{3}{2}} \frac{n_{0e}}{T_{e\perp}\sqrt{T_{e\|}}} \exp\left(-\frac{m_e}{2T_{e\perp}}v_\perp^2 - \frac{m_e}{2T_{e\|}}v_\|^2\right). \quad (2)$$

The electron temperature is presented by $T_{e\perp}$ and $T_{e\|}$ in the directions perpendicular and parallel to the magnetic field, respectively. An electron temperature anisotropy parameter is defined as

$$\Lambda_e = \frac{T_{e\perp}}{T_{e\|}} - 1. \quad (3)$$

Here, $\Lambda_e > 0$ means $T_{e\perp} > T_{e\|}$, and vice versa. Secondly, the electron temperature gradient anisotropy is shown as follows,

$$\omega_*^e = \omega_{*_{e\|}}\left[1 + \frac{1}{2}\eta_{e\|}\left(\frac{m_e v_\|^2}{2T_{e\|}} - 1\right) + \eta_{e\perp}\left(\frac{m_e v_\perp^2}{2T_{e\perp}} - 1\right)\right].$$

Here, $\eta_{e\|}(=L_{ne}/L_{Te\|})$ and $\eta_{e\perp}(=L_{ne}/L_{Te\perp})$ are the electron temperature gradient parameters parallel and perpendicular to the magnetic field, respectively. Meanwhile, $L_{ne}^{-1} = -\mathrm{d}\ln n_e/\mathrm{d}r$, $L_{Te\|}^{-1} = -\mathrm{d}\ln T_{e\|}/\mathrm{d}r$ and $L_{Te\perp}^{-1} = -\mathrm{d}\ln T_{e\perp}/\mathrm{d}r$ are the electron density, electron parallel and perpendicular temperature scale lengths, respectively. In addition, the magnetic field drifts ω_{de},

$$\omega_{de} = \omega_{deB}\left(\frac{v_\perp}{v_{te\|}}\right)^2 + 2\omega_{deC}\left(\frac{v_\|}{v_{te\|}}\right)^2,$$

include the magnetic gradient drift frequency $\omega_{deB}(=k_\theta\rho_{e\|}v_{te\|}/2L_B)$ with the magnetic gradient scale length $L_B^{-1} = -\mathrm{d}\ln B/\mathrm{d}r$, and the magnetic curvature drift frequency $\omega_{deC}(=k_\theta\rho_{e\|}v_{te\|}\varepsilon^2/2q^2\alpha^2 r)$. Moreover, $\omega_{*e\|}(=ck_\theta T_{e\|}/(eBL_{ne}))$ is the electron diamagnetic drift frequency corresponding to the parallel temperature, and $k_\theta = k_\theta\alpha$ is the poloidal wave number.

To derive the nonadiabatic response of trapped electrons, we have to pay attention to two factors. One is the fraction of trapped electrons, which is $\sqrt{2\xi}$ with $\xi = \left(\varepsilon B_{\phi0}^2 + \varsigma B_{\theta0}^2\right)/B_0^2$ in isotropic RFPs, and $\varsigma < \varepsilon$ induces $\xi < \varepsilon$, while B_0, $B_{\phi0}$ and $B_{\theta0}$ are the equilibrium magnetic field in the cylindrical geometry [24]. With regard to the electron temperature anisotropy, the factor is changed to $\sqrt{2\xi(\Lambda_e+1)/(2\Lambda_e\xi+1)}$. It indicates that the fraction of trapped electrons is closely related to the electron temperature anisotropy. The other factor is the trapped electrons' orbit average (i.e. bounce average), which presents in the gyrokinetic equation of trapped electrons. Under the assumption of $\omega \ll \omega_{be}$, where ω_{be} is the electron bounce frequency, the zeroth order term $\delta\tilde{H}_{e0}$ of the trapped electron nonadiabatic response $\delta\tilde{H}_e$ after the bounce average can be written as,

$$\delta\tilde{H}_{e0} = -\sum_{l=-\infty}^{\infty}\int_{2l\pi-\pi}^{2l\pi+\pi} \frac{\left\langle\left(\omega - \omega_*^e\right)\frac{eF_{Me}}{T_{e\|}}\tilde{\phi}\right\rangle}{\langle\omega - \omega_{de}\rangle}\delta\left(\theta - \theta'\right)\mathrm{d}\theta' \quad (4)$$
$$\approx -\frac{\omega - \langle\omega_*^e\rangle}{\omega - \langle\omega_{de}\rangle}\frac{e\langle F_{Me}\rangle}{T_{e\|}}\sum_{l=-\infty}^{\infty}\int_{2l\pi-\pi}^{2l\pi+\pi}\delta\left(\theta-\theta'\right)\mathrm{d}\theta'\langle\tilde{\phi}\rangle,$$

where $\langle\cdots\rangle$ represents the bounce average. It should be noted that the bounce average of the product of three terms in the formula is replaced by the product of three averaged terms, namely, $\langle\omega_*^e F_{Me}\tilde{\varphi}\rangle \approx \omega_*^e F_{Me}\langle\tilde{\varphi}\rangle$. Here, the deeply trapped electron assumption and retention a little $v_\|$ effect are considered [15]. By integrating in the velocity space, the perturbation of the trapped electron density $\tilde{n}_{et}$ is given by

$$\begin{aligned}\tilde{n}_{et} = &-n_{e0}\sqrt{\frac{2\xi}{\pi}}\frac{1}{\Lambda_e+1}\int_0^\infty \mathrm{e}^{-\frac{t}{\Lambda_e+1}}\sqrt{t}\,\mathrm{d}t \\ &\times\int_0^1\frac{\omega - \langle\omega_*^e\rangle}{\omega - \langle\omega_{de}\rangle}G(\kappa^2,t)\frac{\mathrm{d}\kappa^2}{4F(\kappa)} \\ &\times\sum_{j=-\infty}^{\infty}g(\theta-2\pi j,\kappa)\int_{-\infty}^{+\infty}\mathrm{d}\theta' g(\theta',\kappa)\tilde{\phi}(\theta'-2\pi j),\end{aligned} \quad (5)$$

where

$$g(\theta,\kappa) = \int_{-\theta_r}^{\theta_r}\frac{\delta\left(\theta-\theta'\right)\mathrm{d}\theta'}{\sqrt{\kappa^2 - \sin^2\left(\frac{\theta'}{2}\right)}},$$

$$G\left(\kappa^2,t\right) = \frac{\int_0^1\frac{\mathrm{e}^{\left(\frac{1}{\Lambda_e+1}-1\right)2\varepsilon t\kappa^2\left(1-x^2\right)}}{\sqrt{1-x^2}}\frac{\mathrm{d}x}{\sqrt{1-\kappa^2x^2}}}{K(\kappa)}.$$

The other parameters in the function are

$$\begin{aligned}\langle\omega_*^e\rangle = \omega_{*e\|}&\left\{1 - \left(\frac{1}{2}\eta_{e\|} + \eta_{e\perp}\right)\right. \\ &\left.+ 2\eta_{e\|}t\xi H(\kappa) + \frac{1}{\Lambda_e+1}\eta_{e\perp}t[1-2\xi H(\kappa)]\right\},\end{aligned}$$

$$\begin{aligned}\langle\omega_{de}\rangle = \omega_{deB}&\left\{1 + 2\xi\left[1 - \kappa^2 - \frac{F(\kappa)}{K(\kappa)}\right]\right\}t \\ &+ \omega_{deC}\left[4\xi\left(\kappa^2 - 1 + \frac{F(\kappa)}{K(\kappa)}\right)\right]t,\end{aligned}$$

$$H(\kappa) = \left(\kappa^2 - 1\right) + \frac{F(\kappa)}{K(\kappa)}, \quad \kappa^2 = \sin^2\left(\frac{\theta_r}{2}\right).$$

Here, $K(\kappa)$ and $F(\kappa)$ are the complete elliptic integrals of the first and second kinds, respectively, and $t = v^2/v_{te\|}^2$. Meanwhile, θ_r is the returning point in banana orbit for trapped electrons, corresponding to the case where the parallel velocity of the electron is zero. Here, $\delta(x)$ is Dirac's delta function. The theoretical results obtained here will degenerate back to those in isotropic plasmas, when anisotropy reverts to isotropy, $\Lambda_e = 0$, $\eta_{e\perp} = \eta_{e\|}$ [24].

2.2. Ion response

In this work, the ions are treated as isotropic, and the passing ion response, including the full kinetic mechanisms, is considered [22] in RFP plasmas, such as the finite Larmor radius effect, magnetic drifts and plasma inhomogeneity. Based on the quasi-neutrality equation, the integral eigenmode equation for electrostatic perturbation in RFP plasmas is written as,

$$(1+\tau_{\mathrm{i}\|})\hat{\phi}(k) = -\tilde{n}_{\mathrm{e}t} + \int_{-\infty}^{\infty}\frac{\mathrm{d}k'}{\sqrt{2\pi}}\tilde{K}(k,k')\hat{\phi}(k'). \quad (6)$$

The function $\tilde{K}(k,k')$ is related to the nonadiabatic response of ions,

$$\begin{aligned}\tilde{K}\left(k,k'\right) = &-\mathrm{i}\int_{-\infty}^{0}\frac{\omega_{*\mathrm{e}\|}}{\sqrt{2\beta\zeta}}\cdot \mathrm{e}^{-\mathrm{i}\omega\tau}\cdot \mathrm{e}^{-\frac{(k-k')^2}{4\zeta}}\cdot\frac{\mathrm{d}\tau}{\lambda}\\ &\times\left\{\frac{\omega}{\omega_{*\mathrm{e}\|}}\tau_{\mathrm{i}\|}+1-\frac{3}{2}\eta_{\mathrm{i}}+\frac{\eta_{\mathrm{i}}}{\lambda}-\frac{k_\perp^2+k_\perp'^2}{4\lambda^2\tau_{\mathrm{i}\|}}\eta_{\mathrm{i}}\right.\\ &\left.+\eta_{\mathrm{i}}\frac{k_\perp k'_\perp}{2\lambda^2\tau_{\mathrm{i}\|}}\frac{I_1}{I_0}+\eta_{\mathrm{i}}\frac{\left(k-k'\right)^2}{4\beta\zeta}\right\}\Gamma_0\left(k_\perp,k'_\perp\right).\end{aligned} \quad (7)$$

The parameters in the equation are,

$$\lambda = 1+\mathrm{i}\frac{\varepsilon_n}{\varepsilon_B}\frac{\omega_{*\mathrm{e}\|}}{\tau_{\mathrm{i}\|}}\tau, \quad \beta = 1+\mathrm{i}\frac{2\varepsilon\cdot\varepsilon_n}{q^2\alpha^2\tau_{\mathrm{i}\|}}\omega_{*\mathrm{e}\|}\tau,$$

$$\zeta = \frac{\tau^2}{\tau_{\mathrm{i}\|}\beta}\left(\frac{s}{q\alpha}\varepsilon_n\right)^2\omega_{*\mathrm{e}\|}^2, \quad \Gamma_0 = I_0\left(\frac{k_\perp k'_\perp}{2\lambda\tau_{\mathrm{i}\|}}\right)\mathrm{e}^{-\frac{k_\perp^2+k_\perp'^2}{4\lambda\tau_{\mathrm{i}\|}}},$$

$$L_{n\mathrm{i}} = -\left(\frac{\mathrm{d}\ln n_{\mathrm{i}}}{\mathrm{d}r}\right)^{-1} = L_{n\mathrm{e}}, \quad L_{T\mathrm{i}} = -\left(\frac{\mathrm{d}\ln T_{\mathrm{i}}}{\mathrm{d}r}\right)^{-1},$$

$$k_\perp^2 = k_\theta^2+k^2, \quad k_\perp'^2 = k_\theta^2+k'^2, \quad s = \frac{r}{q\alpha}\frac{\mathrm{d}q}{\mathrm{d}r},$$

$$\varepsilon_n = \frac{L_{n\mathrm{e}}}{R}, \quad \varepsilon_B = \frac{L_B}{R}, \quad \eta_{\mathrm{i}} = \frac{L_{n\mathrm{i}}}{L_{T\mathrm{i}}}, \quad \tau_{\mathrm{i}\|} = \frac{T_{\mathrm{e}\|}}{T_{\mathrm{i}}},$$

and $I_l(l=0,1)$ is the modified Bessel function of the order l. More details about the ion response can be found in [21]. Note that different normalizations are used in the two works, such as $\omega\rightarrow\omega_{*\mathrm{e}}$, $\hat{\phi}\rightarrow e\tilde{\phi}/T_{\mathrm{e}}$, and all the wave number $k\rightarrow\rho_s^{-1}$ with $\rho_s = \sqrt{2T_{\mathrm{e}}/m_{\mathrm{i}}}/\Omega_{\mathrm{i}}$ in [21], but $\omega\rightarrow\omega_{*\mathrm{e}\|}$, $\hat{\phi}\rightarrow e\tilde{\phi}/T_{\mathrm{e}\|}$, and all the wave number $k\rightarrow\rho_s^{-1}$ with $\rho_s = \sqrt{2T_{\mathrm{e}\|}/m_{\mathrm{i}}}/\Omega_{\mathrm{i}}$ in this work. All differences are due to the electron temperature anisotropy.

3. Numerical results

The computer code HD7, using the Raleigh–Ritz method to solve the Fredholm homogeneous integral equation of the second, has been modified from isotropic plasmas to anisotropic RFP plasmas. The integral eigenmode equation (6) is then solved numerically with the revised code. The computer algorithm makes HD7 able to discuss the influence of any variable on the drift wave by knowing the values of parameters, such as Λ_{e}, ε_n, η_{i}, η_{e}, k_θ, s and q, but only one variable can be changed at a time. Hence, the radial distributions of quantities are not required in the calculation. The parameters for the numerical results are $\tau_{\mathrm{i}\|} = 1.33, s = 1.0, \eta_{\mathrm{e}} = 5.0, \eta_{\mathrm{i}} = 0, q = 0.15, \varepsilon_n = 0.2, \varepsilon_B = 0.6, \varepsilon = 0.18, \xi = 0.15$ and $k_\theta\rho_s = 0.8$ unless otherwise stated. Note that the acceptable range of Λ_{e} is $-1\leqslant\Lambda_{\mathrm{e}}<\infty$, due to the Λ_{e} definition. Of course, the updated HD7 can also obtain exactly the same numerical solution in isotropic RFP plasmas [24] when $\Lambda_{\mathrm{e}} = 0, \eta_{\mathrm{e}\perp} = \eta_{\mathrm{e}\|} = \eta_{\mathrm{e}}$.

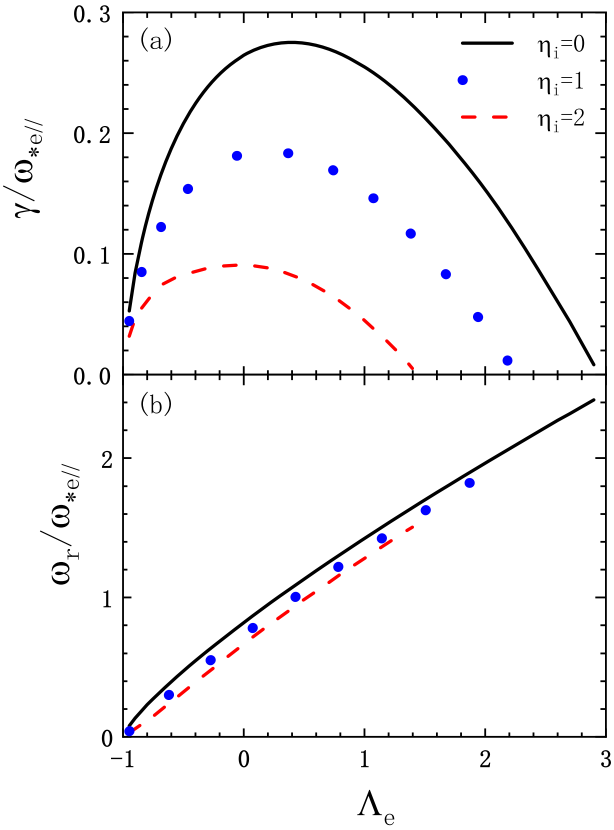

Figure 1. Normalized growth rate (a) and real frequency (b) versus Λ_{e} for different η_{i}.

3.1. Effects of electron temperature anisotropy

Firstly, only the influence of the electron temperature anisotropy on TEM is considered for the isotropic temperature gradient $\eta_{\mathrm{e}\perp} = \eta_{\mathrm{e}\|} = \eta_{\mathrm{e}}$.

Figure 1 shows the normalized growth rate and real frequency of TEM as functions of the electron temperature anisotropy parameter Λ_{e} for different η_{i} values. It should be noted that changing Λ_{e} is equivalent to changing only $T_{\mathrm{e}\perp}$, because $\tau_{\mathrm{i}\|} = T_{\mathrm{e}\|}/T_{\mathrm{i}}$ is fixed in the calculation, indicating that $T_{\mathrm{e}\|}$ is constant. Figure 1(a) shows that TEM instability enhances first and then weakens with the increase in$T_{\mathrm{e}\perp}$. There is a critical value of Λ_{e}, corresponding to the turning point of TEM instability from enhancing to weakening. Here, the enhancement of TEM instability results from the increase in the trapped electron fraction, i.e. the fraction for a positive Λ_{e} is bigger than that in the isotropic case, $\sqrt{2\xi(\Lambda_{\mathrm{e}}+1)/(2\Lambda_{\mathrm{e}}\xi+1)}>\sqrt{2\xi}$. On the other hand, the

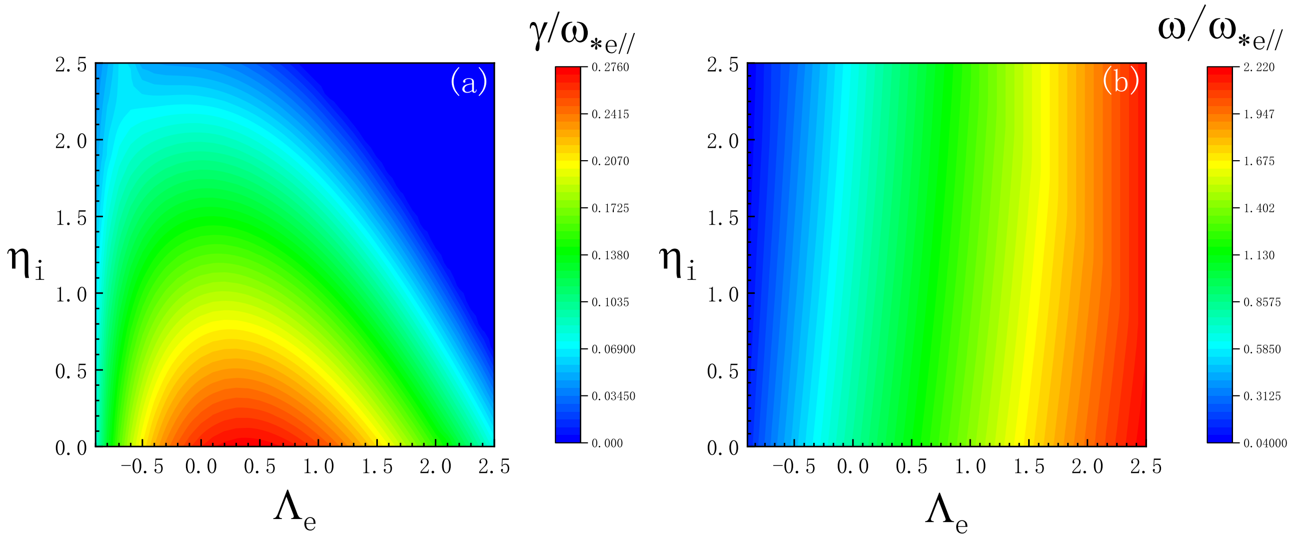

Figure 2. Normalized growth rate (a) and real frequency (b) versus η_i and Λ_e spectrum.

weakening of the instability comes from two aspects: one is the stronger Landau damping, the other is the energy conservation. In figure 1(*b*), the real frequency of TEM ω_r increases quickly and approximately linearly with increasing Λ_e, which indicates that Landau damping increases quickly with increasing Λ_e. Within the context of energy conservation, the bigger $T_{e\perp}$ means a smaller $T_{e\parallel}$. When Λ_e is large enough, the trapped electrons with relatively low parallel velocity restrict the scale of bounce movement, resulting in the weakening of TEM instability. Similar phenomena have been found in tokamak theory [15] and experiments after ECRH [16]. On the other hand, the critical value of Λ_e depends on η_i, such as $\Lambda_e \approx 0.38, 0.2$ and -0.05 at $\eta_i = 0, 1$ and 2, respectively. Interestingly, the critical value of Λ_e is smaller and smaller with increasing η_i, but it is just the opposite in tokamak plasmas. The stronger Landau damping in an RFP can explain this phenomenon. For TEM, η_i plays a stabilizing role in both RFP and tokamak plasmas. With the combination of the rapidly increasing Landau damping caused by bigger Λ_e and the stabilizing effect of η_i, the turning point of Λ_e gradually moves to the small Landau damping at smaller positive Λ_e, even for negative Λ_e. However, the results in tokamak plasmas [15] show that the real frequency of TEM increases very slowly in a certain Λ_e region, which means the increase in Landau damping is very small. Even when the η_i effect is taken into account, the effect of the trapped electron fraction on TEM destabilization is dominant. The real frequency begins to increase rapidly when positive Λ_e is big enough, resulting in rapid stabilization of TEM with larger Landau damping in a tokamak. Therefore, the stronger Landau damping in an RFP makes the critical value of Λ_e appear earlier than that in a tokamak.

Figure 2 further proves the above conclusions, where a two-dimensional graph of normalized growth rate and real frequency changing with Λ_e and η_i is plotted. It is clearly shown that η_i has a stabilization effect on TEM for a fixed Λ_e, regardless of whether $T_{e\parallel} \geqslant T_{e\perp}$ or $T_{e\parallel} < T_{e\perp}$, which is similar to the results for the isotropic case [24]. Moreover, a big positive Λ_e causes a narrow η_i region for the instability. Similarly, the negative Λ_e enlarges the η_i region for TEM instability with smaller Landau damping. In addition, a bigger positive η_i makes the critical value of Λ_e become smaller, and is consistent with the results of figure 1. However, η_i has a little influence on the real frequency at a fixed Λ_e, as shown by the fact that the values of the real frequency in figure 2(*b*) change slowly for a fixed Λ_e, suggesting that η_i has a minor effect on the Landau damping for both isotropic and anisotropic RFP plasmas.

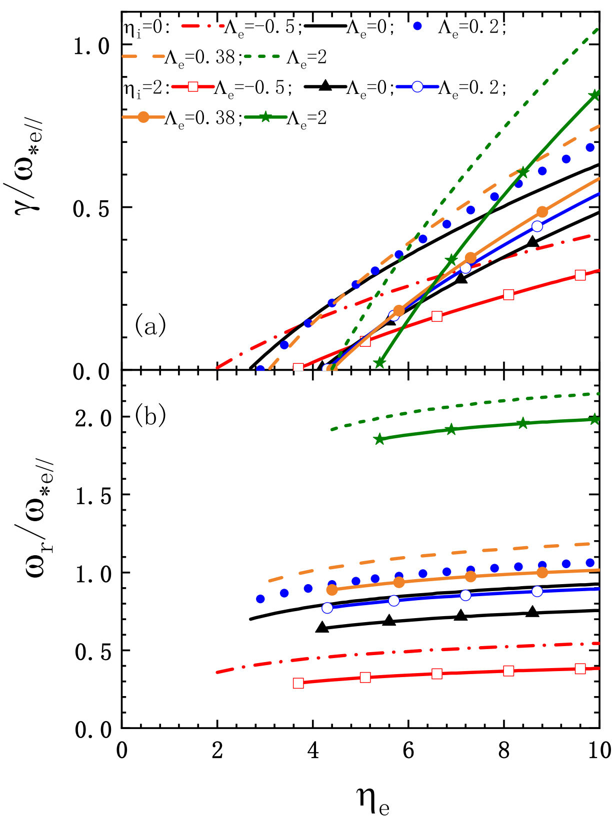

Figure 3. Normalized growth rate (a) and real frequency (b) versus η_e for different Λ_e and η_i.

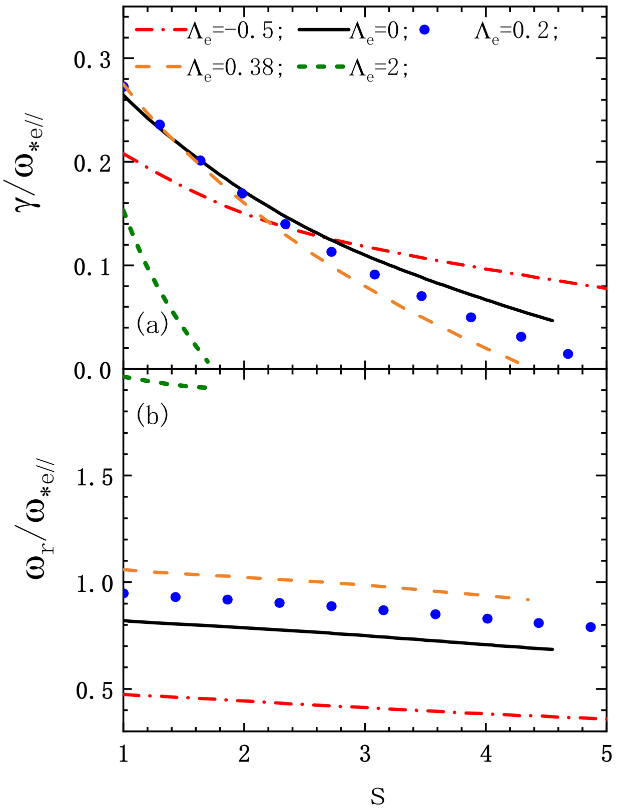

Figure 4. Normalized growth rate (a) and real frequency (b) versus s for different Λ_e.

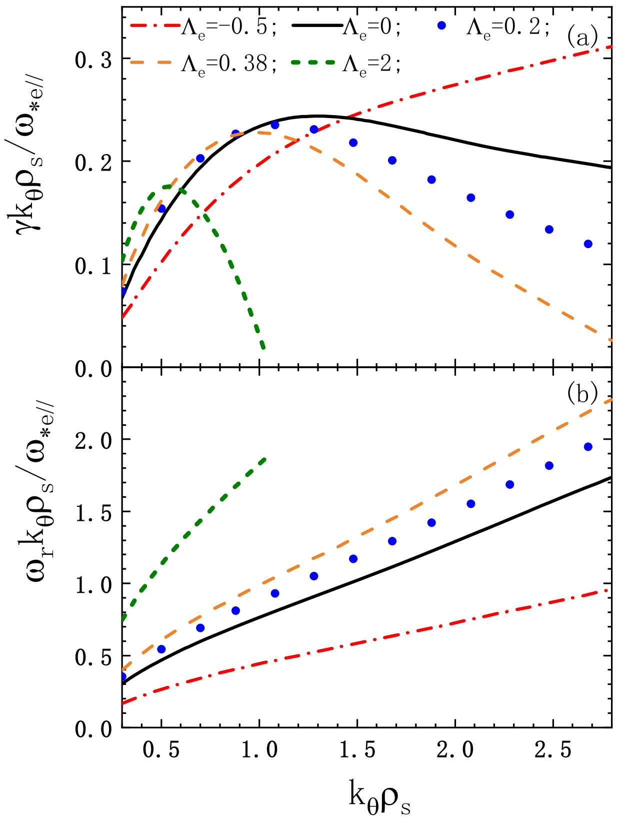

Figure 5. Normalized growth rate (a) and real frequency (b) versus $k_\theta \rho_s$ for different Λ_e.

Next, the η_e effect on TEM is plotted in figure 3, which shows that η_e makes TEM unstable, even for anisotropic plasmas as expected. The higher the η_e, the larger the driving force on TEM is. Of course, it is necessary to excite the TEM with a bigger η_e for a big η_i, which has stabilizing effect on TEM. The electron temperature anisotropy affects the η_e threshold of TEM excitation, such that a negative Λ_e reduces the η_e threshold for exciting TEM instability. As shown in figure 3(*a*), the red dash–dot lines for $\Lambda_e = -0.5$ appear at a smaller η_e compared with other lines for a fixed η_i. In contrast, for a large positive Λ_e, a bigger η_e is needed to excite TEM. However, it is conducive to the growth rate of the instability increases with increasing η_e more rapidly larger Λ_e, where the enhancing of the trapped electron fraction by positive Λ_e plays an important role. Meanwhile, the Landau damping is relatively less affected by η_e, as shown by the slow change in real frequency in figure 3(*b*).

The effect of magnetic shear on TEM with temperature anisotropy is studied in figure 4. The results follow the normal conclusion that the magnetic shear has an overall stabilizing effect on microturbulence [36], even for anisotropic RFP plasmas. The positive Λ_e amplifies the stabilizing effect of magnetic shear on TEM, so TEM tends to become stable more quickly with the increase in positive Λ_e, and vice versa. It indicates that the free energy of the trapped electrons in the perpendicular direction is more easily dissipated by magnetic shear; thus, it decreases TEM instability. In addition, the critical Λ_e is 0.38 at $\eta_i = 0$; therefore, the growth rate for $\Lambda_e = 2$ is smaller than that for $\Lambda_e = 0.38$ and decays faster. In contrast, the higher parallel electron temperature with smaller Landau damping enlarges the TEM unstable s region. It also shows that the critical Λ_e is related to magnetic shear.

The k_θ spectra for electron temperature anisotropy are presented in figure 5, where a new normalization ($\omega \to \omega^*_{e\parallel}/k_\theta \rho_s$) has been employed to remove $k_\theta \rho_s$ from $\omega_{*e\parallel}$. Neglecting the η_i stabilizing effect, the influences of negative and positive Λ_e are different. TEM is weakened with increasing k_θ when the electron temperature in the perpendicular direction is higher than that in the parallel direction, especially for $k_\theta \rho_s > 1$. Moreover, TEM is strongly stabilized by the bigger positive Λ_e for higher k_θ. This phenomenon is opposite to the results in a tokamak [15], where the TEM instability increases with increasing k_θ for any Λ_e. In RFP plasmas, only a negative Λ_e gives rise to an overall destabilizing effect on TEM with increasing k_θ. As mentioned above, a negative Λ_e induces a smaller Landau damping effect in RFP plasmas; thus, the rate of the real frequency change with $k_\theta \rho_s$ in figure 5(*b*) is less than that for positive Λ_e. The driving force for the modes of short wavelength is greater than the whole Landau damping for negative Λ_e, leading to the same TEM results in RFP and tokamak plasmas (i.e. TEM is more unstable at the shorter wavelength). Therefore, the Landau damping plays a dominant role in TEM in RFP plasmas. On the other hand, the red dash–dot lines ($\Lambda_e = -0.5$) are higher or lower than other curves at different $k_\theta \rho_s$, indicating that the critical value of Λ_e is closely related to the wavelength. The smaller the wavelength, the closer to

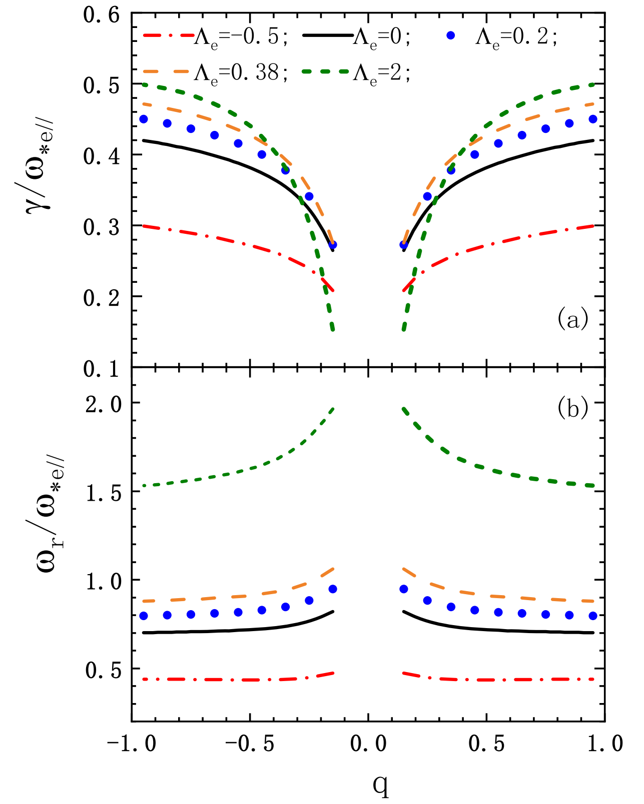

Figure 6. Normalized growth rate (a) and real frequency (b) versus q for different Λ_{e}.

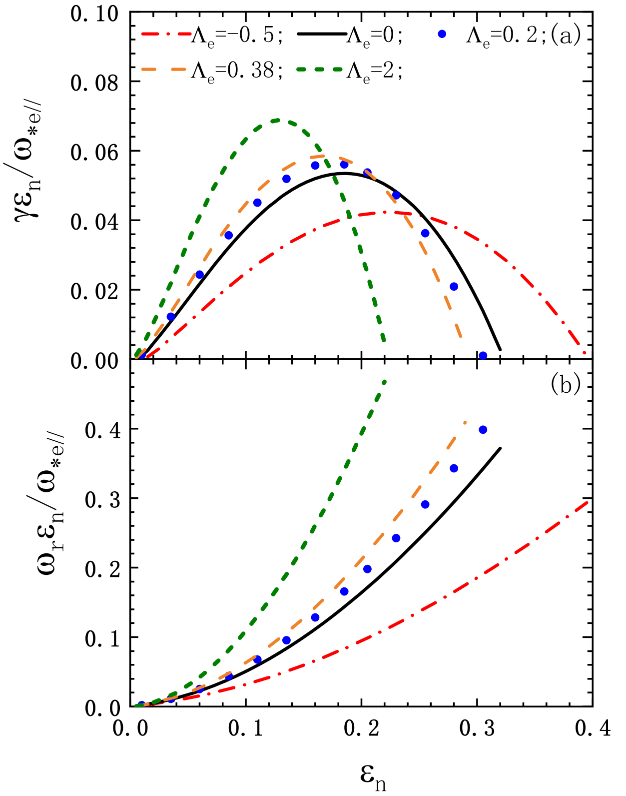

Figure 7. Normalized growth rate (a) and real frequency (b) versus ε_n for different Λ_{e}.

the negative Λ_{e} region the turning point of Λ_{e} is, as shown in figure 1.

The safety factor q in RFP plasmas is small, positive or negative. The effects of q on TEM are given in figure 6 for different Λ_{e}. The results are symmetrical for positive and negative q, which is consistent with the square form of q in equation (6). In addition, the bigger $|q|$ is helpful for the destabilization of TEM instability for any Λ_{e}, especially for a bigger Λ_{e}, such as $\Lambda_{\mathrm{e}} = 2$, since the real frequency and Landau damping for the bigger Λ_{e} are reduced with increasing $|q|$, i.e. the Landau damping is weakened at large $|q|$. This is also different from that observed in tokamak plasmas [15], where the increase in q obviously reduces the instability of TEM for large and positive Λ_{e} with $q > 1$. On the other hand, q also has an effect on the Λ_{e} critical value, such that the results for $\Lambda_{\mathrm{e}} = -0.5$ and $\Lambda_{\mathrm{e}} = 2$ are opposite on the two sides of $q = 0.2$. Therefore, the bigger the safety factor, the higher the positive Λ_{e} turning point is.

The influence of density gradient scale length on TEM in plasmas of electron temperature anisotropy is shown in figure 7, where a new normalization is employed to remove ε_n in $\omega_{*\mathrm{e}\|}$. As expected, the steeper and flatter density profiles provide stronger and weaker driving forces for TEM instability, respectively. The electron temperature anisotropy magnifies these effects. The higher $T_{\mathrm{e}\perp}$ raises the trapped electron fraction to make TEM unstable in the small ε_n region. However, the enhancement of Landau damping reduces TEM instability with the increasing ε_n. Although the higher $T_{\mathrm{e}\|}$ weakens the driving force for TEM in a small ε_n region, it enlarges the ε_n region of unstable TEM, and even TEM instability in a fairly flat density distribution. The negative Λ_{e} with smaller Landau damping is the reason for this expanded TEM instability in the big ε_n region. Moreover, the turning point of Λ_{e} is also related to ε_n, and the ε_n effect is also included in η_{i} and η_{e}.

3.2. Effects of electron temperature gradient anisotropy

The anisotropy of electron temperature and its gradient is studied in this section.

Figures 8 and 9 show the normalized growth rate and real frequency of TEM as functions of $\eta_{\mathrm{e}_\perp}$ (fixing $\eta_{\mathrm{e}_\|} = 5$) and $\eta_{\mathrm{e}_\|}$ (fixing $\eta_{\mathrm{e}_\perp} = 5$), respectively. The numerical results show some very interesting phenomena. Firstly, $\eta_{\mathrm{e}\|}$ and $\eta_{\mathrm{e}\perp}$ can both drive TEM instability in an RFP. This is different from that in a tokamak [15], where $\eta_{\mathrm{e}\|}$ has a stabilizing effect on TEM. In comparison, the driving force of the perpendicular temperature gradient $\eta_{\mathrm{e}\perp}$ is stronger. TEM instability exists at $\eta_{\mathrm{e}\perp} = 5$ and $\eta_{\mathrm{e}\|} = 0$ in figure 9(*a*), except for when $\Lambda_{\mathrm{e}} = 2$, while the growth rate is zero at $\eta_{\mathrm{e}\perp} = 0$ and $\eta_{\mathrm{e}\|} = 5$ in figure 8(*a*). This means that even if there is no $\eta_{\mathrm{e}\|}$, the perpendicular temperature gradient can drive the TEM instability alone; therefore, the driving force in the perpendicular direction is stronger. The analysis of real frequency can explain this phenomenon, where $\eta_{\mathrm{e}\perp}$ and $\eta_{\mathrm{e}\|}$ decrease and increase the real frequency, corresponding to weakening and enhancement of Landau damping, respectively. In addition, the strong Landau damping and the weak driving effect of $\eta_{\mathrm{e}\|}$ reduce TEM instability in the bigger $\eta_{\mathrm{e}\|}$ region. As shown in figure 9(*a*), the growth rate decreases with increasing $\eta_{\mathrm{e}\|}$ after exceeding a

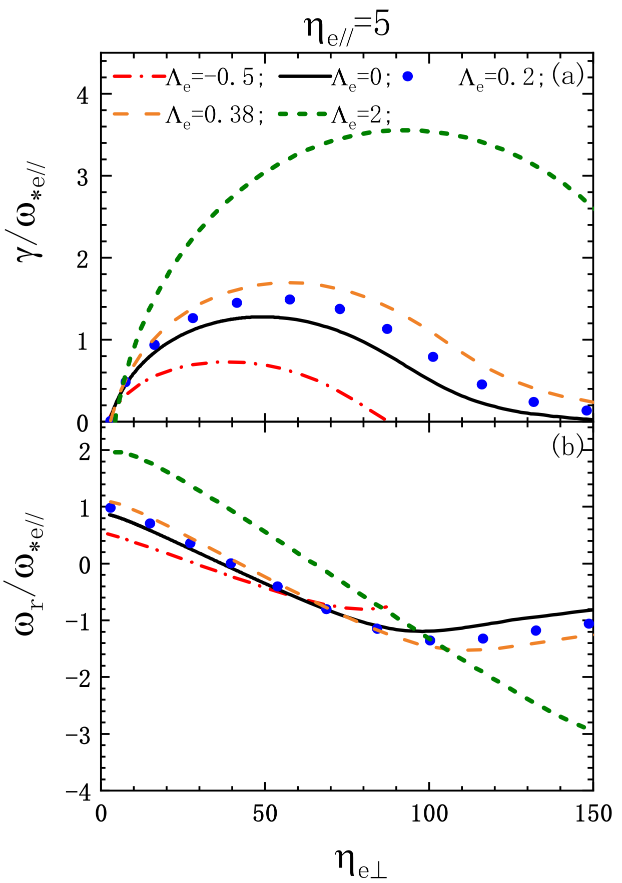

Figure 8. Normalized growth rate (a) and real frequency (b) versus $\eta_{e_\perp}$.

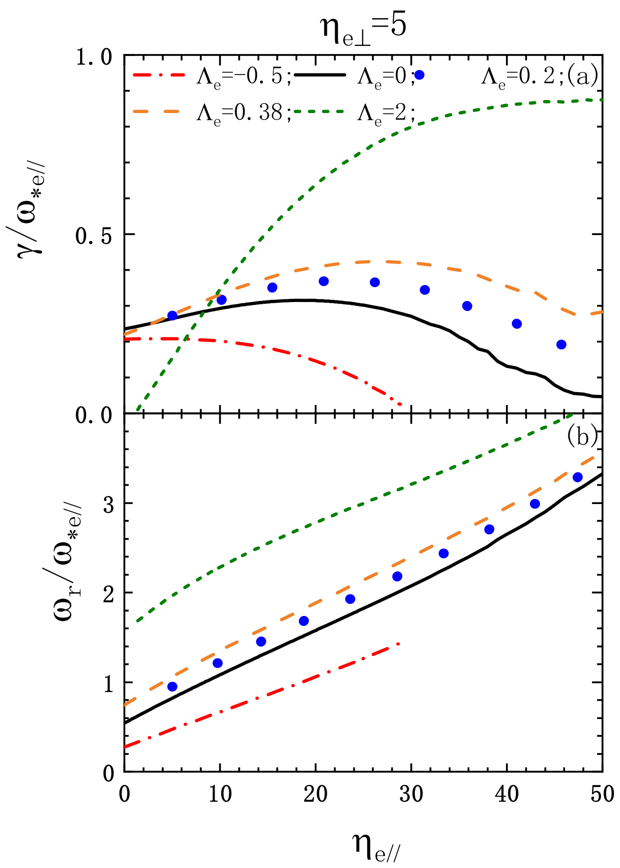

Figure 9. Normalized growth rate (a) and real frequency (b) versus $\eta_{e_\parallel}$.

certain $\eta_{e\parallel}$. Secondly, there is a positive correlation between temperature anisotropy and temperature gradient anisotropy. TEM is more unstable for the bigger anisotropies of temperature and its gradient, and vice versa. As mentioned above, a higher positive Λ_e causes stronger Landau damping, so a large temperature gradient is needed to excite TEM instability. The green-dashed lines show the features of this. For example, the TEM instability occurs at $\eta_{e\parallel} \approx 1.6$ in figure 9(*a*) and $\eta_{e\perp} \approx 5$ in figure 8(*a*), respectively. As for the excitation of TEM instability, a bigger anisotropy of electron temperature with gradient rapidly increases TEM instability. Finally, an electron–ion hybrid mode is present when $\eta_{e\perp}$ is extremely large, such as $\eta_{e\perp} > 38.4, 49.2, 53, 57$ and 92 for $\Lambda_e = -0.5, 0, 0.2, 0.38$ and 2 in figure 9(*a*), respectively. It is not the standard TEM or ITG mode, because the real frequency changes from positive to negative continuously in the region of $\eta_{e\perp}$. A similar phenomenon is found in tokamak theory [15] and experiments [16], but the occurrence point of $\eta_{e\perp}$ is several times smaller than that of $\eta_{e\perp}$ in RFPs. The anisotropy of electron temperature synchronization enlarges or reduces the occurrence point $\eta_{e\perp}$; therefore the hybrid mode is more likely to appear in higher $T_{e\parallel}$ RFP plasmas.

3.3. Electron temperature gradient threshold

In this section, the influence of electron temperature anisotropy on the electron temperature gradient threshold for excitation of TEM is studied and compared with that in isotropic RFP plasmas. Here, the anisotropy of the electron temperature gradient is neglected for simplicity, corresponding to $\eta_{e\perp} = \eta_{e\parallel} = \eta_e$.

Figure 10 shows the relation between the electron density gradient ε_n and temperature gradient threshold $\varepsilon_{T\mathrm{th}}(\varepsilon_T = L_{Te}/R = \varepsilon_n/\eta_e)$ of TEM excitation. Every curve divides the graph into two parts. TEM is stable and unstable in the regions above and below the curve, respectively. In comparison with isotropic plasmas ($\Lambda_e = 0$), TEM is more difficult to excite for positive Λ_e in the big ε_n region, but is easier to excite for negative Λ_e, even for flat density profiles. This seems to contradict with the former results in that the higher $T_{e\perp}$ can help to enhance the trapped electron fraction and then increase TEM instability. In fact, the former results also show that a positive Λ_e offers stronger Landau damping, especially the bigger the positive Λ_e, the stronger the Landau damping is. The temperature gradient threshold corresponds to the smallest driving force for TEM instability. Therefore, TEM instability is easy to excite in the case of negative Λ_e due to weaker Landau damping, while it needs a steeper temperature profile when $\Lambda_e > 0$. Therefore, the negative Λ_e results in a bigger unstable TEM region, and Landau damping plays a dominant role in the temperature gradient threshold of TEM excitation. On the other hand, once TEM instability is excited, a positive Λ_e increases the trapped electrons fraction, leading to the effective enhancement of unstable TEM, while TEM instability increases slowly when $\Lambda_e < 0$ because of the smaller fraction of trapped electrons. Hence, the conclusion obtained here is consistent

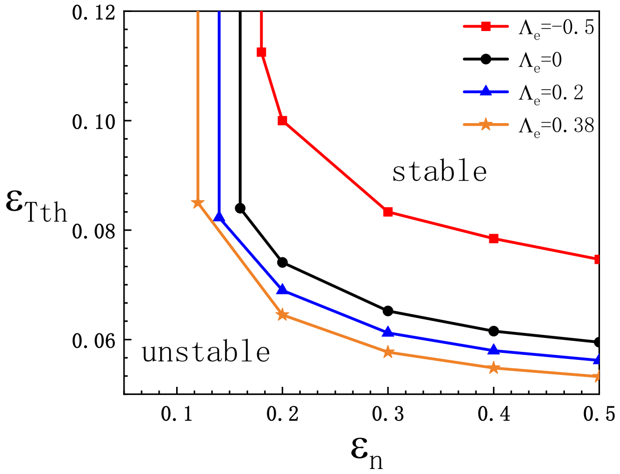

Figure 10. The temperature gradient threshold $\varepsilon_{T\mathrm{th}}$ versus density gradient ε_n for different Λ_e. The other parameters are the same as those used in figure 1, except $\eta_\mathrm{i} = 0$ here.

with the former results. Figure 3(*a*) also confirms the results here, where TEM instability always appears first at small η_e in the case of negative Λ_e when η_i is fixed, but the growth rate of TEM with positive Λ_e increases much faster than that with negative Λ_e. Although positive Λ_e increases the temperature gradient threshold required to excite TEM instability, the steeper temperature profile has been detected in the edge of RFP experiments [37]. This means that TEM may be excited at the edge of RFP experiments. In addition, the left regions of the vertical lines indicate that TEMs can be excited without the temperature gradient ($\varepsilon_{T\mathrm{th}} \to \infty$), and the steep enough density profile, such as $\varepsilon_n < 0.12$, can fully excite TEM instability. The anisotropy of electron temperature also increases or decreases the required minimum ε_n.

4. Conclusion and discussion

A gyrokinetic integral eigenmode equation to describe the effect of anisotropic electron temperature and its gradient on TEM is derived in toroidal RFP plasmas. Results from systematic numerical analyses are presented. The main conclusions are as follows. (1) The anisotropy of electron temperature enhances TEM instability when the temperature in the direction perpendicular to the magnetic field is higher than that in the parallel direction ($\Lambda_\mathrm{e} > 0$). However, this enhancement is limited, and there is a critical Λ_e, corresponding to the turning point of TEM instability from enhancing to weakening, which is related to the fact that the strong Landau damping plays an important role in RFP plasmas. Moreover, the critical Λ_e depends on the plasma parameters, such as η_i, η_e, ε_n, q, s and $k_\theta\rho_s$. (2) Electron temperature anisotropy does not change the basic effects of η_i, η_e, s, $k_\theta\rho_s$, q and ε_n on TEMs, but only enhances/weakens them. For example, a positive/negative Λ_e enhances/reduces the stabilizing effect of s on TEM. (3) The electron temperature gradients in the perpendicular and parallel directions both drive TEM instability, while the driving force of $\eta_{\mathrm{e}\perp}$ is stronger. In addition, an electron–ion hybrid mode appears when $\eta_{\mathrm{e}\perp}$ is big enough, just like that found in tokamaks. (4) A negative Λ_e enlarges the TEM unstable region, which means that the higher electron temperature in the parallel direction is helpful for the excitation of TEM instability, where Landau damping has a dominant effect on TEM excitation.

In this work, only the influence of anisotropic electron temperature and its gradient on TEM has been discussed. We also need to pay more attention to the effect of plasma anisotropy on microturbulence-induced transport. In addition, a circular cross-section of plasmas is assumed to obtain the eigenmode equation. Although the Keda Torus eXperiment (KTX) experiment is a circular cross-section, other RFP experimental devices have produced a magnetic configuration with a non-circular cross-section, such as a divertor configuration; therefore, the non-circular section is an interesting topic for the future. Moreover, here we only concentrate on the linear effect of TEM in anisotropic RFP plasmas. Its nonlinear effects, such as TEM-driven zonal flows that tend to regulate turbulence transport, and bootstrap current characteristics (in particular, when the perpendicular electron temperature is higher than that in the parallel direction, it induces an increase in the trapped electron fraction, resulting in an increase in the bootstrap current fraction), are more meaningful topics for one to understand physics and to be beneficial to RFP experiments.

Acknowledgments

This work was supported by the National Key R & D Program of China under Grant No. 2017YFE0301702, and the National Science Fund for Talent Training in the Basic Sciences (No. J1103208).

ORCID iDs

W. Kong https://orcid.org/0000-0002-5165-9855
J.C. Li https://orcid.org/0000-0001-9918-8880

References

[1] Horton W. 1999 *Rev. Mod. Phys.* **71** 735
[2] Tang W.M. 1978 *Nucl. Fusion* **18** 1089
[3] Pierrard V., Lazar M., Poedts S., Štverák Š., Maksimovic M. and Trávníček P.M. 2016 *Sol. Phys.* **291** 2165
[4] Pustovitov V.D. and Stepanyan S.A. 2011 *Plasma Phys. Control. Fusion* **53** 035004
[5] Pustovitov V.D. 2011 *Plasma Phys. Rep.* **37** 109
[6] Laqua H.P., Moseev D., Helander P., Aleynikov P., Marsen S., Maruschenko N.B. and Stange T. 2018 *Nucl. Fusion* **58** 104003
[7] Wu M.Q. *et al* 2019 *Nucl. Fusion* **59** 106009
[8] Neuner U. *et al* 2003 *Nucl. Fusion* **61** 036024
[9] Nagamine Y. *et al* 2003 *AIP Conf. Proc.* **669** 589
[10] Choe W., Chang C.S. and Ono M. 1995 *Phys. Plasmas* **2** 2044
[11] Mathey O. and Sen A.K. 1989 *Phys. Rev. Lett.* **62** 268
[12] Song H. and Sen A.K. 1993 *Phys. Fluids* B **5** 2806
[13] Dong J.Q., Long Y.X. and Avinash K. 2001 *Phys. Plasmas* **8** 4120
[14] Jia M.X., Li J.C., Liu S.F., Kong W., Zhu K.E. and Dong J.Q. 2021 *Nucl. Fusion* **61** 046033

[15] Yao Y., Liu S.F., Zhu K.E., Kong W., Li J.Q. and Dong J.Q. 2022 *Nucl. Fusion* **62** 036027
[16] Qin Z., Imadera K., Li J. and Kishimoto Y. 2018 *Plasma Fusion Res.* **13** 3403083
[17] Lorenzini R. *et al* 2009 *Nat. Phys.* **5** 570
[18] Chapman B.E. *et al* 2001 *Phys. Rev. Lett.* **87** 205001
[19] Sasaki K. *et al* 1997 *Plasma Phys. Control. Fusion* **39** 333–8
[20] Den Hartog D.J. and Craig D. 2000 *Plasma Phys. Control Fusion* **42** L47
[21] Guo S.C. 2008 *Phys. Plasmas* **15** 122510
[22] Liu S., Guo S.C. and Dong J.Q. 2010 *Phys. Plasmas* **17** 052505
[23] Liu S.F., Guo S.C., Zhang C.L., Dong J.Q., Carraro L. and Wang Z.R. 2011 *Nucl. Fusion* **51** 083021
[24] Liu S.F., Guo S.C., Kong W. and Dong J.Q. 2014 *Nucl. Fusion* **54** 043006
[25] Carmody D., Pueschel M.J. and Terry P.W. 2013 *Phys. Plasmas* **20** 052110
[26] Sattin F., Garbet X. and Guo S.C. 2010 *Plasma Phys. Control. Fusion* **52** 105002
[27] Predebon I. and Xanthopoulos P. 2015 *Phys. Plasmas* **22** 052308
[28] Predebon I., Sattin F., Veranda M., Bonfiglio D. and Cappello S. 2010 *Phys. Rev. Lett.* **105** 195001
[29] Carmody D., Pueschel M.J., Anderson J.K. and Terry P.W. 2015 *Phys. Plasmas* **22** 012504
[30] Williams Z.R., Pueschel M.J., Terry P.W. and Hauff T. 2017 *Phys. Plasmas* **24** 122309
[31] Duff J.R., Williams Z.R., Brower D.L., Chapman B.E., Ding W.X., Pueschel M.J., Sarff J.S. and Terry P.W. 2018 *Phys. Plasmas* **25** 010701
[32] Gao Z., Dong J.Q., Liu G.J. and Ying C.T. 2003 *Phys. Plasmas* **10** 774
[33] Dong J.Q., Horton W. and Kim J.Y. 1992 *Phys. Fluids* B **4** 1867
[34] Dong J. 2018 *Plasma Sci. Technol.* **20** 094005
[35] Holod I. and Lin Z. 2013 *Phys. Plasmas* **20** 032309
[36] Burrell K.H. 1997 *Phys. Plasmas* **4** 1499
[37] Frassinetti L., Alfier A., Pasqualotto R., Bonomo F. and Innocente P. 2008 *Nucl. Fusion* **48** 045007